Journal of Alloys and Compounds 525 (2012) 191–201

Contents lists available at SciVerse ScienceDirect

Journal of Alloys and Compounds

journal homepage: www.elsevier.com/locate/jallcom

Critical systematic evaluation and thermodynamic optimization of the Mn–RE system: RE = La, Ce, Pr, Nd and Sm

Junghwan Kim, In-Ho Jung*

Department of Mining and Materials Engineering, McGill University, 3610 University St., Montreal, Quebec H3A 2B2, Canada

ARTICLE INFO

Article history:
Received 9 December 2011
Received in revised form 7 February 2012
Accepted 8 February 2012
Available online xxx

Keywords:
Thermodynamic modeling
Phase diagrams
Thermodynamic properties
Modified Quasichemical Model
Compound Energy Formalism

ABSTRACT

Critical evaluation and optimization of all available phase diagram and thermodynamic data for the Mn–RE (RE = La, Ce, Pr, Nd and Sm) systems have been conducted to obtain reliable thermodynamic functions of all the phases in the system. In the thermodynamic modeling, it is found that the Mn–RE systems show systematic changes in the phase diagrams and thermodynamic properties such as enthalpy of mixing in liquid state in the order of periodic number in the lanthanide series. This systematic thermodynamic modeling approach for all light RE elements can allow to resolve inconsistencies in the experimental data.

1. Introduction

Rare Earth (RE) metals are widely used in many industrial fields including permanent magnet, electronic materials and structural materials. As a small addition of RE can enhance magnetic, electronic, optical and mechanical properties of numerous materials, the usage of the RE is still expanding regardless of the strategic control of their supply.

Magnesium alloys are getting great scientific and industrial attention as the lightest structural materials. One of the drawbacks of Mg alloys is their poor formability at room temperature due to the limited slip system with hcp crystal structure. Recently, several studies [1–5] show that the additions of small amounts of RE can considerably enhance the ductility of Mg alloys. Therefore, a lot of research on Mg–RE alloys is undergoing to clarify the role of RE on the enhanced deformation mechanism and to find out the most optimum Mg alloy compositions. In order to respond to the need of Mg–RE alloy development, a large thermodynamic database for Mg alloys containing RE has been developed with critical systematic analysis and optimization of the entire RE series data. This includes the thermodynamic database of the Mg–RE [6], Mg–RE–RE [6], Mg–Al–RE [7,8], Mg–Zn–RE and Mg–Mn–RE systems.

In the thermodynamic "optimization" of a chemical system, all available thermodynamic and phase equilibrium data are evaluated simultaneously in order to obtain one set of model equations for the Gibbs energies of all phases as functions of temperature and composition. From these equations, all the thermodynamic properties and phase diagrams can be back-calculated. In this way, all the data are rendered self-consistent and consistent with thermodynamic principles. Thermodynamic property data, such as activity data, can aid in the evaluation of the phase diagram, and phase diagram measurements can be used to deduce thermodynamic properties. Discrepancies in the available data can often be resolved, and interpolations and extrapolations can be made in a thermodynamically correct manner.

Recently, the thermodynamic optimizations for several binary Mn–light RE systems have been performed. The Mn–Ce system was optimized by Tang et al. [9] and Kang et al. [10], and the Mn–Pr and Mn–Sm systems were optimized by Wang et al. [11,12]. No thermodynamic optimizations have been conducted for the Mn–La and Mn–Nd systems. In addition, new enthalpy of mixing data for liquid Mn–Sm and Mn–Nd systems were determined very recently by Berezutskii and Ivanov [13] and Ivanov et al. [14], respectively, which can be critical to constrain the thermodynamic properties of the systems. The entalapy prediction by the previous optimization by Wang et al. [12] for the Mn–Sm system is completely inconsistent with these new experiemntal data by Berezutskii and Ivanov [13].

Therefore, the primary purpose of the present study is to perform a complete review of all available experimental data and previous optimizations and critical optimization of thermodynamic properties of alloy phases in binary Mn–light RE alloy systems. In particular, the systematic analysis of the whole light RE systems can provide a more accurate evaluation of the thermodynamic

* Corresponding author. Tel.: +1 514 398 2608; fax: +1 514 398 4492.
E-mail address: in-ho.jung@mcgill.ca (I.-H. Jung).

0925-8388/$ – see front matter.
doi:10.1016/j.jallcom.2012.02.072

properties and phase diagram data of Mn–RE. The Mn–Pm and Mn–Eu systems were not considered in the present study because no thermodynamic and phase diagram data are available in the literature although Pm and Eu are in the light RE class. This study is part of the thermodynamic database development of multicomponent Mg–RE alloy design.

2. Thermodynamic models

2.1. Liquid phase

The Modified Quasichemical Model [15,16], which accounts for short-range-ordering of nearest-neighbor atoms, was used to model the liquid solutions because it gives a more realistic thermodynamic description of the liquid phase compared with the conventional simple random-mixing Bragg Williams model [15,16]. The Modified Quasichemical Model was successfully applied to many liquid metallic solutions [16–18] and ionic solutions [19,20] exhibiting strong short-range-ordering behavior.

Recently, the energy of nearest-neighbor pair formation in the Modified Quasichemical Model is expanded as a polynomial in the pair fractions [15,16] instead of the component fractions [19,21]. In addition, the coordination numbers are now allowed to vary with composition. These modifications provide greater flexibility in reproducing the binary experimental data and in combining optimized binary liquid parameters into a large database for multicomponent solutions [15]. A short description of the model is given below; details can be found in previous studies [15,16].

In the case of a binary *A*–*B* liquid solution, the atoms *A* and *B* are distributed over the sites of a quasi-lattice in liquid solution. The following pair exchange reaction can be considered:

$$(A-A)+(B-B)=2(A-B) \tag{1}$$

where $(A-B)$ represents a first-nearest-neighbor pair of *A* and *B*. The non-configurational Gibbs energy change for the formation of two moles of $(A-B)$ pairs according to reaction [1] is Δg_{AB}. Then the Gibbs energy of the solution is given by:

$$G=(n_A G_A^o+n_B G_B^o)-T\Delta S^{config}+n_{AB}\left(\frac{\Delta g_{AB}}{2}\right) \tag{2}$$

where G_A^o and G_B^o are the molar Gibbs energies of the pure components *A* and *B*, n_A and n_B are the numbers of moles of *A* and *B* atoms, and n_{AB} is the number of moles of $(A-B)$ pairs. ΔS^{config} is the configurational entropy of mixing given by a random distribution of the $(A-A)$, $(B-B)$ and $(A-B)$ pairs in the one-dimensional Ising approximation:

$$\Delta S^{\text{config}}=-R(n_A\ \ln X_A+n_B\ \ln X_B)-R\left[n_{AA}\ \ln\left(\frac{X_{AA}}{Y_B^2}\right)\right.$$
$$\left.+n_{BB}\ \ln\left(\frac{X_{BB}}{Y_B^2}\right)+n_{AB}\ \ln\left(\frac{X_{AB}}{2Y_AY_B}\right)\right] \tag{3}$$

where n_{AA}, n_{BB} and n_{AB} are the numbers of moles of each kind of pairs, and the pair fraction (X_{AA}, X_{BB} and X_{AB}) and coordination equivalent fraction (Y_A and Y_B) can be calculated as:

$$X_{AA}=\frac{n_{AA}}{n_{AA}+n_{BB}+n_{AB}} \tag{4}$$

$$X_{BB}=\frac{n_{BB}}{n_{AA}+n_{BB}+n_{AB}} \tag{5}$$

$$X_{AB}=\frac{n_{AB}}{n_{AA}+n_{BB}+n_{AB}} \tag{6}$$

$$Y_A=\frac{X_{AA}+X_{AB}}{2} \tag{7}$$

$$Y_B=\frac{X_{BB}+X_{AB}}{2} \tag{8}$$

The Δg_{AB} is the model parameter to reproduce the Gibbs energy of liquid phase of the binary $A-B$ system, which is expanded as a polynomial in terms of the pair fractions, as follows:

$$\Delta g_{AB}=\Delta g_{AB}^o+\sum_{i\geq 1}g_{AB}^{i0}(X_{AA})^i+\sum_{j\geq 1}g_{AB}^{0j}(X_{BB})^j \tag{9}$$

where Δg_{AB}^o, g_{AB}^{i0} and g_{AB}^{0j} are the adjustable model parameters which can be functions of temperature.

In the Modified Quasichemical Model, the coordination numbers of *A* and *B*, Z_A and Z_B, can be varied with composition to reproduce the short-range-ordering as follows:

$$\frac{1}{Z_A}=\frac{1}{Z_{AA}^A}\left(\frac{2n_{AA}}{2n_{AA}+n_{AB}}\right)+\frac{1}{Z_{AB}^A}\left(\frac{n_{AB}}{2n_{AA}+n_{AB}}\right) \tag{10}$$

$$\frac{1}{Z_B}=\frac{1}{Z_{BB}^B}\left(\frac{2n_{BB}}{2n_{BB}+n_{AB}}\right)+\frac{1}{Z_{BA}^B}\left(\frac{n_{AB}}{2n_{BB}+n_{AB}}\right) \tag{11}$$

where Z_{AA}^A is the value of Z_A when all nearest neighbors of an *A* atom are *A* atoms, and Z_{AB}^A is the value of Z_A when all nearest neighbors are *B* atoms. Z_{BB}^B and Z_{BA}^B are defined in an analogous manner. In the present study, Z_{ii}^i for all elements (i = Mn and RE (La, Ce, Pr, Nd and Sm)) are set to be 6. To reproduce the maximum or minimum enthalpies of Mn–light RE liquid alloys at 0.3–0.4 mol fraction RE, $Z_{\text{MnRE}}^{\text{Mn}}$ and $Z_{\text{MnRE}}^{\text{RE}}$ are set to be 3 and 6, respectively. During the course of the present study, it was found that this set of coordination numbers can reproduce the experimental data more accurately with a small number of model parameters. For example, if the coordination numbers of Mn and RE for all nearest neighbors were set to 6, more model parameters would have been required and the experimental data would have been less accurately reproduced.

2.2. Solid solutions

The solid solution phases were described by the Compound Energy Formalism [22] with a one-sublattice approach (Mn, RE) for substitutional site. The molar Gibbs energy of the solid solution can be expressed as:

$$G=(y_{\text{Mn}}G_{\text{Mn}}^o+y_{\text{RE}}G_{\text{RE}}^o)+RT(y_{\text{Mn}}\ \ln y_{\text{Mn}}+y_{\text{RE}}\ \ln y_{\text{RE}})$$
$$+{}^aL_{\text{Mn,RE}}y_{\text{Mn}}y_{\text{RE}}(y_{\text{RE}}-y_{\text{Mn}})^a \tag{12}$$

where y_{Mn} and y_{RE} are the site fractions of Mn and RE elements in the sublattice, and *R* and *T* are the gas constant and temperature in Kelvin. G_{Mn}^o and G_{RE}^o are the molar Gibbs energies of solid phases of Mn and RE. The binary interaction parameters between Mn and RE in the sublattice, ${}^aL_{\text{Mn,RE}}$ where $a\geq 0$, are adjustable models parameters.

2.3. Stoichiometric compounds and elements

The Gibbs energies of all pure elements are taken from the SGTE database version 5.0 [23]. As the heat capacities of all stoichiometric compounds in Mn–light RE systems were not available, they were estimated using the Neumann–Kopp rule. There is no experimental study for the enthalpy and entropy of formation at 298 K of the intermetallic compounds in Mn–light RE systems. Consequently, the enthalpy and entropy of formation at 298 K were used as adjustable parameters to reproduce the phase diagram of the systems.

BCC (Mn), FCC (Mn) and $Mn_{23}Sm_6$ phases in Mn–light RE systems exhibit magnetic transitions associated with Neel or Curie temperatures. The magnetic transition below 298 K (typically antiferromagnetic transition with Neel temperature) was taken directly

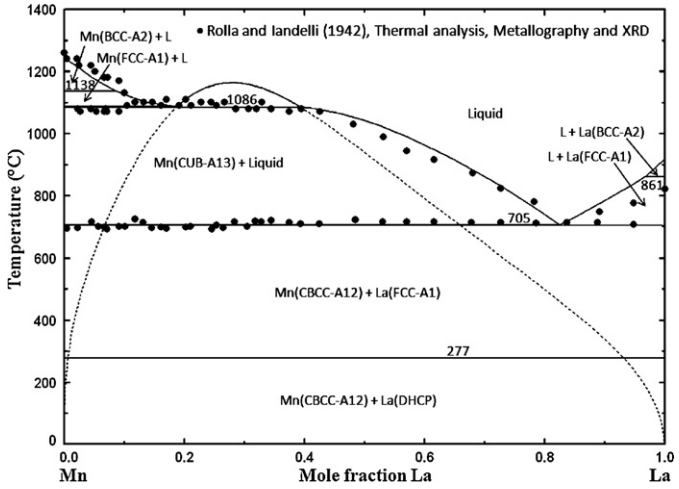

Fig. 1. The optimized phase diagram of the Mn–La system with experimental data [27].

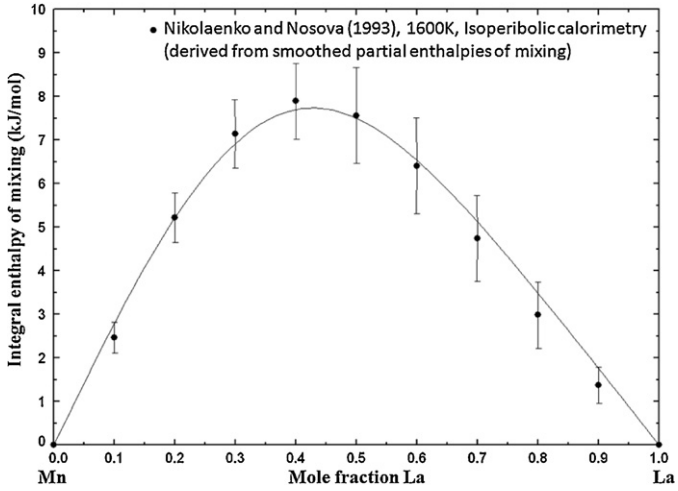

Fig. 2. Integral enthalpy of mixing in Mn–La liquid at 1600 K with experimental data [28].

into account in the calculation of S_{298}. The Curie temperature (ferromagnetic transition) occurs typically above 298 K, of which magnetic contribution to the Gibbs energy was considered by an empirical relationship suggested by Inden [24] and modified by Hillert and Jarl [25].

3. Critical evaluation and thermodynamic optimization

The thermodynamic optimizations of the binary systems were performed based on all available thermodynamic data for the compounds, solid and liquid solutions and on the critically assessed phase diagram data. The optimized values for the model parameters are listed in Table 1. The details of the thermodynamic optimization are explained in the following sections. All the thermodynamic calculations were performed using the FactSage thermodynamic software [26].

3.1. The Mn–La system

The only available experimental phase diagram for this system was investigated by Rolla and Iandelli [27] using thermal analysis (TA) followed by metallography and X-ray diffraction (XRD) in the entire composition range. The alloys were prepared from 99.5 wt.% La and 99.8 wt.% Mn in Pythagoras crucibles under a melt of NaCl + $BaCl_2$ in a Tamann furnace. The monotectic and eutectic reactions were observed at 1081 °C and 701 °C, respectively, using TA. The existence of a liquid miscibility gap was found from a thermal arrest detected at 1081 °C in the composition range of 0.6–0.85 mol fraction La. However, the consolute temperature of the binary miscibility gap was not determined. No intermediate phases were found in the system. Using XRD, the authors also proposed no mutual solubility of La and Mn in the solids. The phase diagram data of Rolla and Iandelli [27] are shown in Fig. 1.

Nikolaenko and Nosova [28] determined the partial enthalpy of mixing of La between $0 < X_{La} < 0.63$ and that of Mn between $0.48 < X_{La} < 1.0$ at 1600 K in liquid Mn–La using isoperibolic calorimetry and starting materials made of 99.9 wt.% Mn and 99.86 wt.% La. Then, using the Gibbs–Duhem equation, they suggested smoothed values of both, the partial enthalpies of mixing and the integral enthalpy of mixing, in the whole Mn–La liquid. The experimental data of the partial and integral enthalpies of the liquid are presented in Figs. 2 and 3, respectively. The integral enthalpy of mixing of the Mn–La liquid shows a positive deviation from ideal solution behavior with a maximum at about 8 kJ mol^{-1} near 0.4 mol fraction La.

The system was previously assessed by Palenzona and Cirafici [29] using only the experimental data of Rolla and Iandelli [27], for which the melting temperature of La and the liquidus were modified. In our optimization, the temperature-independent terms of the liquid interaction parameters were firstly adjusted to reproduce the experimental enthalpy data of Figs. 2 and 3. However, the parameters were insufficient to reproduce the phase diagram data of Fig. 1. Consequently, the calculated phase diagram and enthalpies were well reproduced after adding small temperature-dependent model parameters as shown in Figs. 1–3. The only remaining discrepancies are observed for the La liquidus though. Its melting temperature reported by Rolla and Iandelli [27] is already lower than the accepted melting temperature by about 100 °C. The reason of the experimental error cannot be clarified, but it may be associated to the strong oxidation behavior of La. The calculated invariant reactions are listed in Table 2 in comparison with the experimental ones. The calculated consolute temperature of the binary miscibility gap is 1165 °C at 0.28 mol fraction La.

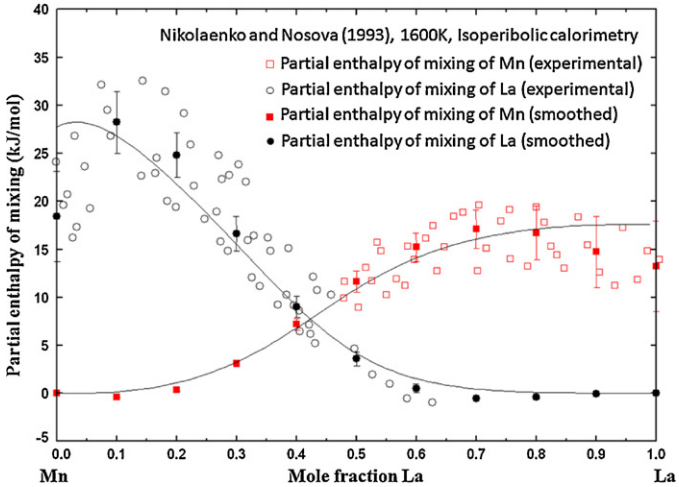

Fig. 3. Partial enthalpies of mixing in Mn–La liquid at 1600 K with experimental data [28].

Table 1
Optimized model parameters for the all binary systems (J mol^{-1} or J mol^{-1} K^{-1}).

Phase	Thermodynamic parameters			
Liquid	Coordination numbers			
	i	j	Z^i_{ij}	Z^j_{ij}
	Mn	La	3	6
	Mn	Ce	3	6
	Mn	Pr	3	6
	Mn	Nd	3	6
	Mn	Sm	3	6
	$\Delta g_{MnLa} = 15{,}062.4 - 7.1128T + (-2092.0 + 4.6024T)X_{MnMn}$			
	$+ (-3347.2 + 0.8368T)X_{LaLa} - 3765.6\,X^2_{MnMn}$			
	$\Delta g_{MnCe} = 5439.2 - 0.8368T - 1673.6\,X^2_{MnMn}$			
	$\Delta g_{MnPr} = 5020.8 - 0.523T - 627.6\,X_{PrPr}$			
	$\Delta g_{MnNd} = 2092 - 1.883T$			
	$+ (-4184 + 6.276T)X_{MnMn} + (4184 + 0.335T)\,X_{NdNd}$			
	$\Delta g_{MnSm} = 1673.6 + 2.51T + (-418.4 + 2.51T)X_{MnMn}$			
	$+ (3347.2 - 2.72T)X_{SmSm} + 4184\,X^2_{SmSm}$			
FCC-A1 (Mn, Ce)	${}^0L_{Mn,Ce} = 27, 519.4$, ${}^1L_{Mn,Ce} = 2173.96$			
	$T^{FCC\text{-}A1}_{C,Mn}$ (Curie temperature) = 540 K, $B^{FCC\text{-}A1}_{O,Mn}$ (Magnetic moment) = 0.62 μ_B mol^{-1}, P factor = 0.28			
BCC-A2 (Mn, Ce, Pr, Nd)	${}^0L_{Mn,Ce} = 22, 812.24$, ${}^1L_{Mn,Ce} = -1915.28$			
	${}^0L_{Mn,Pr} = 41, 840$, ${}^1L_{Mn,Pr} = -39, 748 + 4.184T$,			
	${}^2L_{Mn,Pr} = 50, 208 - 38.074T$			
	${}^0L_{Mn,Nd} = 41, 840$, ${}^1L_{Mn,Nd} = -34, 727.2 + 4.184T$,			
	${}^2L_{Mn,Nd} = 50, 208 - 38.074T$			
	$T^{BCC\text{-}A2}_{C,Mn} = 580$ K, $B^{BCC\text{-}A2}_{O,Mn} = 0.27\,\mu_B$ mol^{-1}, P factor = 0.4			
CUB-A13 (Mn)	$G^{CUB\text{-}A13}_{Ce} = G^{FCC\text{-}A1}_{Ce} + 2510.4$			
	${}^0L_{Mn,Ce} = 20, 920 + 5.02T$			
DHCP (Pr)	$G^{DHCP}_{Mn} = G^{CBCC\text{-}A12}_{Mn} + 2000$			
	${}^0L_{Mn,Pr} = 31, 380$			
$Mn_{23}Pr_6$	$\Delta H^O_{298} = 130, 047.88$, $S^O_{298} = 1326.34$			
	$C_p = 23 \times C_p$ (Mn, CBCC-A12) + $6 \times C_p$ (Pr, DHCP)			
$Mn_{23}Nd_6$	$\Delta H^O_{298} = 113, 453.68$, $S^O_{298} = 1318.16$			
	$C_p = 23 \times C_p$ (Mn, CBCC-A12) + $6 \times C_p$ (Nd, DHCP)			
Mn_2Nd	$\Delta H^O_{298} = 16, 202.94$, $S^O_{298} = 156.05$			
	$C_p = 2 \times C_p$ (Mn, CBCC-A12) + C_p (Nd, DHCP)			
$Mn_{23}Sm_6$	$\Delta H^O_{298} = -42, 000$, $S^O_{298} = 1186.09$			
	$C_p = 23 \times C_p$ (Mn, CBCC-A12) + $6 \times C_p$ (Sm, RHOMB)			
	$T_c = 439$ K, $B_0 = 3\,\mu_B$ mol^{-1} [47], P factor = 0.28			
Mn_2Sm	$\Delta H^O_{298} = -6300$, $S^O_{298} = 136.90$			
	$C_p = 2 \times C_p$ (Mn, CBCC-A12) + C_p (Sm, RHOMB)			

Table 2
Calculated invariant reactions with the experimental data in the Mn–La system.

Type	Reaction	T (°C)	Reference
Monotectic	$L(X_{La} = 0.187) \rightarrow Mn(CUB\text{-}A13, X_{La} = 0) + L(X_{La} = 0.392)$	1086.2	This work[21]
	$L(X_{La} = 0.122) \rightarrow Mn(CUB\text{-}A13, X_{La} = 0) + L(X_{La} = 0.392)$	1081.0	
Eutectic	$L(X_{La} = 0.825) \rightarrow Mn(CBCC\text{-}A12, X_{La} = 0) + La(FCC\text{-}A1, X_{La} = 1)$	705.3	This work[21]
	$L(X_{La} = 0.830) \rightarrow Mn(CBCC\text{-}A12, X_{La} = 0) + La(FCC\text{-}A1, X_{La} = 1)$	701.0	

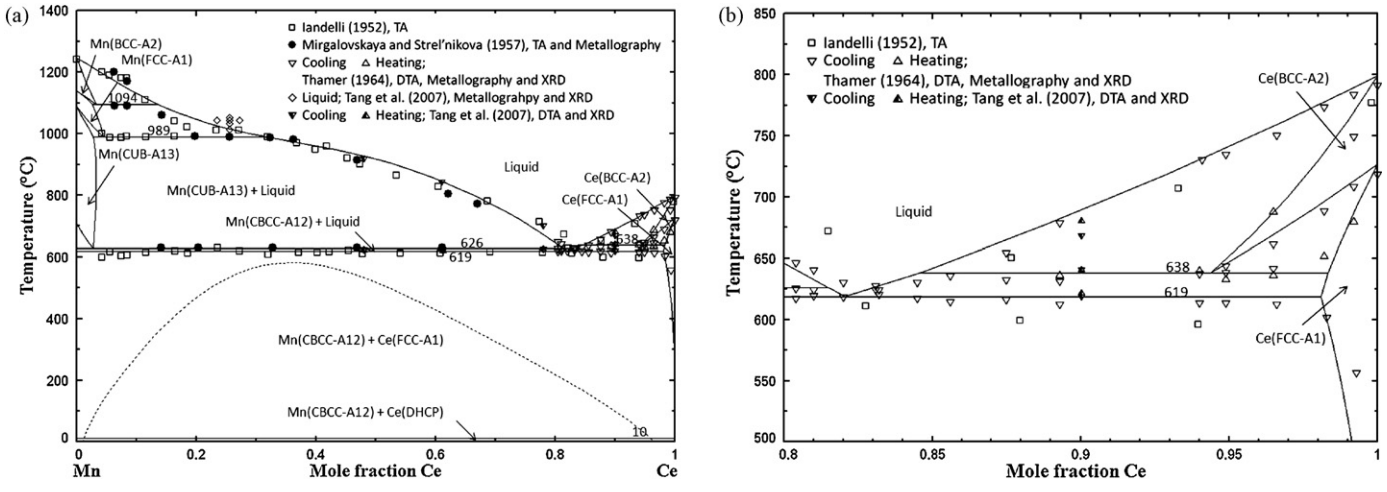

Fig. 4. The optimized phase diagram of the Mn–Ce system in whole composition range (a) and in the range of 0–20 mol% Mn (b) with experimental data [9,30–33].

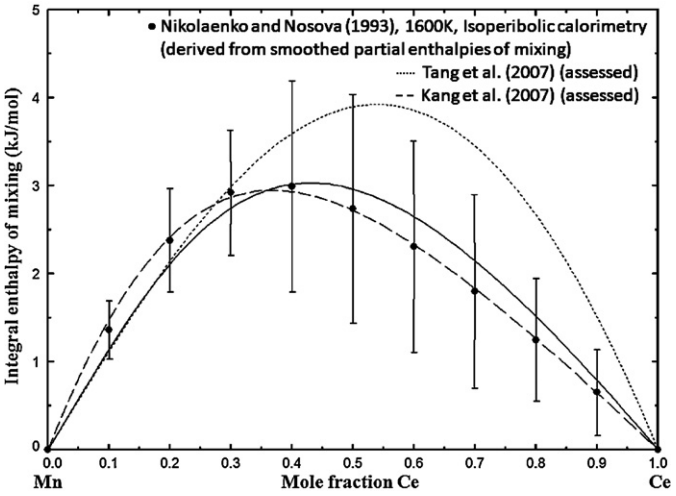

Fig. 5. Integral enthalpy of mixing in Mn–Ce liquid at 1600 K with experimental data [28]. The previous optimizations of Tang et al. [9] and Kang et al. [10] are depicted by the dotted line and dashed line, respectively.

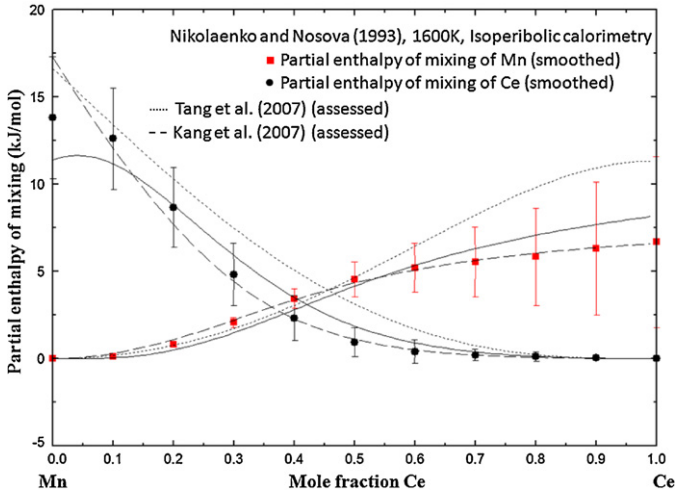

Fig. 6. Partial enthalpies of mixing in Mn–Ce liquid at 1600 K with experimental data [28]. The previous optimizations of Tang et al. [9] and Kang et al. [10] are depicted by the dotted line and dashed line, respectively.

3.2. The Mn–Ce system

An early investigation of the phase diagram was carried out by Iandelli [30] using TA with alloys made from 99.5 wt.% Ce and 99.8 wt.% Mn. The eutectic reaction was located at 0.85 mol fraction Ce at 612 °C while a possible liquid miscibility gap with a monotectic between 0.18 and 0.324 mol fraction Ce at 998 °C was reported. No intermediate solid phases were detected. Mirgalovskaya and Strel'nikova [31] reinvestigated the system using TA and metallography and agreed reasonably well with the work of Iandelli [30] except for the eutectic temperature at 635 °C. Mirgalovskaya and Strel'nikova assumed that the allotropic transition temperatures of Mn at 998 °C and 1087 °C, which are different from those of pure Mn, were due to some solid solubility of Ce in Mn (BCC and FCC). Thamer [32] determined the phase diagram by DTA, metallography and XRD in the Ce-rich region between 500 and 800 °C with starting materials having a higher purity than those of Iandelli [30]. The eutectic reaction was positioned at 0.84 mol fraction Ce at 622 °C. The solubility of Mn in Ce was determined to be about 5 mol% Mn in Ce (BCC) and about 2 mol% Mn in Ce (FCC) at 638 °C. Later, Tang et al. [33] prepared several alloys in the liquid miscibility gap region assumed by Iandelli [30] and confirmed the non-existence of immiscibility by XRD and scanning electron microscopy (SEM) analysis from the quenched samples. Afterwards, Tang et al. [9] prepared four key alloys by arc melting using 99.9 wt.% Mn and Ce, respectively, for key experiments to support their thermodynamic modeling. Samples were annealed at 600 °C and identified by XRD. Phase transition temperatures were determined by DTA using alumina crucibles under Ar atmosphere. Results agree well with other experimental data, which are depicted in Fig. 4.

Nikolaenko and Nosova [28] measured the partial enthalpy of mixing of Mn in the Ce-rich region and that of Ce in the Mn-rich region of the Mn–Ce liquid at 1600 K using isoperibolic calorimetry and starting materials made of 99.9 wt.% Mn and 99.86 wt.% Ce. Then, based on the Gibbs–Duhem equation, they proposed smoothed values of both, the partial and the integral enthalpies of mixing, for the entire Mn–Ce liquid. Unlike the Mn–La system, they only showed smoothed values without any experimental data. The experimental data of the partial and integral enthalpies of the liquid are presented in Figs. 5 and 6, respectively. The integral enthalpy of mixing of the Mn–Ce liquid shows positive deviation from ideal solution behavior with a maximum at about 3 kJ mol^{-1} near 0.4 mol fraction Ce, which is less than half of the Mn–La system.

The system was previously assessed by Palenzona and Cirafici [34] based mainly on the work of Iandelli [30], Mirgalovskaya and Strel'nikova [31] and Thamer [32] and reviewed by Okamoto [35]. Recently, thermodynamic optimizations were performed by Tang et al. [9] and Kang et al. [10]. Unfortunately, the optimization of Kang et al. [10] omitted the solubility of Mn in Ce determined by Thamer [32]. In the thermodynamic optimization of Tang et al. [9], the authors adopted the Bragg–Williams random mixing model with the Redlich–Kister expression for the liquid. However, they did not consider the thermodynamic data of the liquid phase determined by Nikolaenko and Nosova [28]. The calculated integral and partial enthalpies of mixing for the liquid phase at 1600 K optimized by Tang et al. [9] are slightly off from the experimental data of Nikolaenko and Nosova [28]; this is shown in Figs. 5 and 6.

In the present thermodynamic modeling, the mutual solubilities of Mn and Ce in both, FCC-A1 and BCC-A2 solid solutions, were reproduced with two temperature-independent Gibbs excess parameters with the assumption of large solid state miscibility gaps. The solubility of Ce in Mn CUB-A13 solid solution was estimated using its liquidus and the transition temperatures of Mn CUB-A13 to Mn FCC-A1 and Mn CBCC-A12 to Mn CUB-A13, respectively. The eutectic temperature determined by Thamer [32] (622 °C) and Tang et al. [9] (621 °C) were considered as the eutectic temperature of L → Ce FCC-Al solid solution + Mn CBCC-A12. The Gibbs energy of Ce in Mn CUB-A13 structure is assessed to be 2.5104 kJ mol^{-1} relative to the stable structure of Ce FCC-A1 since the stable Ce CUB-A13 is not available. No solid solution was considered for the Mn CBCC-A12 phase because no solubility data exist for this phase. For the liquid, a small temperature dependent term was needed to reproduce both, the phase diagram and enthalpy data, of the liquid phase. The computed phase diagram and the partial and integral enthalpies of the liquid are in good agreement with the experimental data, which is shown in Figs. 4–6. In the phase diagram of Fig. 4a, the metastable liquid miscibility gap is depicted as a dotted line. The calculated invariant reactions are compared to the experimental ones in Table 3.

3.3. The Mn–Pr system

Saccone et al. [36] investigated the complete phase diagram using DTA, metallography, XRD and electron probe micro-analysis (EPMA). The alloys were prepared in the induction furnace using starting materials made of 99.9 wt.% Pr and 99.9 wt.% Mn and

Table 3
Calculated invariant reactions with the experimental data in the Mn–Ce system.

Type	Reaction	T (°C)	Reference
Catatectic	Mn(BCC-A2, X_{Ce} = 0.033) → Mn(FCC-A1, X_{Ce} = 0.027) + L(X_{Ce} = 0.136)	1094.0	This work
	Mn(BCC-A2, X_{Ce}[a]) → Mn(FCC-A1, X_{Ce}[a]) + L(X_{Ce} = 0.130)	1087.0	[25]
Catatectic	Mn(FCC-A1, X_{Ce} = 0.044) → Mn(CUB-A13, X_{Ce} = 0.028) + L(X_{Ce} = 0.314)	989.4	This work
	Mn(FCC-A1, X_{Ce}[a]) → Mn(CUB-A13, X_{Ce}[a]) + L(X_{Ce} = 0.175)	998.0	[25]
Catatectic	Mn(CUB-A13, X_{Ce} = 0.028) → Mn(CBCC-A12, X_{Ce} = 0) + L(X_{Ce} = 0.815)	626.2	This work
	Mn(CUB-A13, X_{Ce}[a]) → Mn(CBCC-A12, X_{Ce}[a]) + L(X_{Ce} = 0.835)	625.0	[26]
Catatectic	Ce(BCC-A2, X_{Ce} = 0.944) → Ce(FCC-A1, X_{Ce} = 0.983) + L(X_{Ce} = 0.846)	637.8	This work
	Ce(BCC-A2, X_{Ce} = 0.95) → Ce(FCC-A1, X_{Ce} = 0.98) + L(X_{Ce} = 0.86)	638.0	[26]
	Ce(BCC-A2, X_{Ce}[a]) → Ce(FCC-A1, X_{Ce}[a]) + L(X_{Ce}[a])	640.0	[28]
Eutectic	L(X_{Ce} = 0.821) → Mn(CBCC-A12, X_{Ce} = 0) + Ce(FCC-A1, X_{Ce} = 0.981)	618.7	This work
	L(X_{Ce} = 0.850) → Mn(CBCC-A12, X_{Ce} = 0) + Ce(FCC-A1, X_{Ce} = 1)	612.0	[24]
	L(X_{Ce} = 0.878) → Mn(CBCC-A12, X_{Ce} = 0) + Ce(FCC-A1, X_{Ce}[a])	635.0	[25]
	L(X_{Ce} = 0.839) → Mn(CBCC-A12, X_{Ce} = 0) + Ce(FCC-A1, X_{Ce}[a])	622.0	[26]
	L(X_{Ce}[a]) → Mn(CBCC-A12, X_{Ce}[a]) + Ce(FCC-A1, X_{Ce}[a])	621.0	[28]

[a] The exact compositions are not specified in the reference.

tantalum or molybdenum crucibles which were sealed by welding to prevent the oxidation and evaporation of sample. The authors reported the existence of the $Mn_{23}Pr_6$ compound, which forms peritectically at 790 °C and decomposes at about 650 °C, after verifying the quenched samples by EPMA and corresponding powders by XRD. They also confirmed that the metastable Laves-type $PrMn_2$ phase forms peritectically at 740 °C and disappears to form Pr_6Mn_{23} after annealing for a few hours at temperatures slightly below 740 °C. Using DTA, it was proposed that the solubilities of Mn in Pr BCC and Pr DHCP at 665 °C are about 6 mol% Mn and 1–2 mol% Mn, respectively. Moreover, the solubility of Pr in Mn was shown to be negligible based on EPMA results. The phase transformation temperature of Mn CBCC-A12 to Mn CUB-A13 was detected at 600 °C by DTA (cooling path), which is much lower than the accepted allotropic transformation of Mn (707 °C). Apparently, this difference is due to the slow kinetics of the transformation in the solid state and therefore these experimental data were not taken into account in the present optimization. The experimental data of Saccone et al. [36] are presented in Fig. 7.

Nikolaenko and Nosova [28] measured the partial enthalpy of mixing of Mn in the Pr-rich region and that of Pr in the Mn-rich region of Mn–Pr liquid at 1600 K using isoperibolic calorimetry and starting materials made of 99.9 wt.% Mn and 99.86 wt.% Pr. Like in the previous two Mn–RE systems, they proposed smoothed values of both, the partial and the integral enthalpies of mixing, for the whole Mn–Ce liquid using the Gibbs–Duhem equation. Unfortunately, they also gave only smoothed values without any experimental data. The enthalpy data are presented in Figs. 8 and 9. The Mn–Pr liquid has a slightly lower positive enthalpy of mixing than the Mn–Ce liquid. The maximum in the integral enthalpy of mixing curve is about 2.5 kJ mol^{-1} near 0.4 mol fraction Pr.

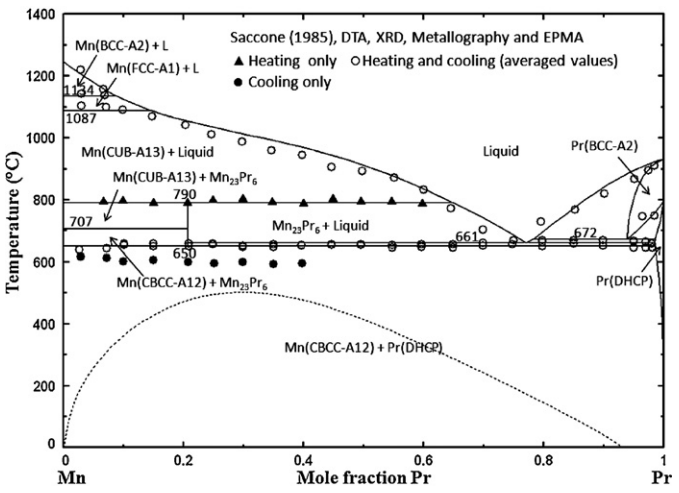

Fig. 7. The optimized phase diagram of the Mn–Pr system with experimental data [36].

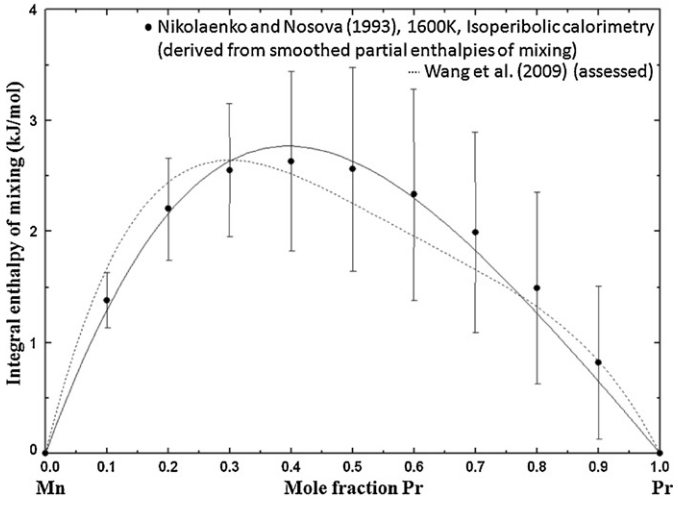

Fig. 8. Integral enthalpy of mixing in Mn–Pr liquid at 1600 K with experimental data [28]. The dotted line shows the previous optimization of Wang et al. [11].

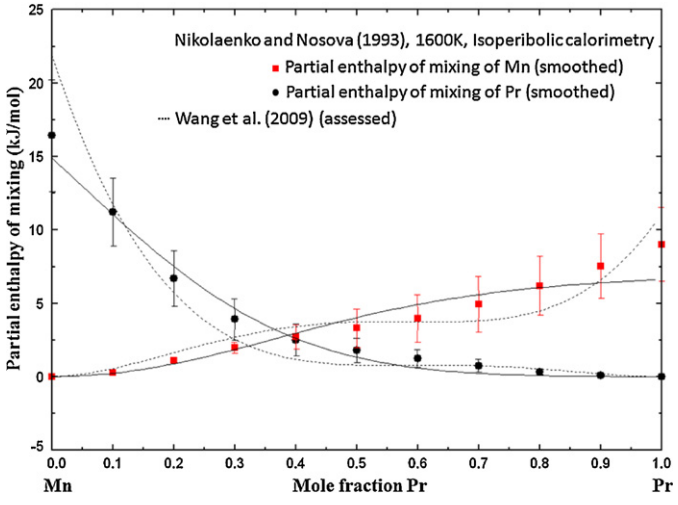

Fig. 9. Partial enthalpies of mixing in Mn–Pr liquid at 1600 K with experimental data [28]. The previous optimization of Wang et al. [11] is depicted by the dotted line.

Previous optimization for this system was performed by Wang et al. [11] using a random-mixing model for the liquid phase. Although Wang et al. could reproduce the experimental data of the phase diagram, the calculated integral and partial enthalpies of mixing of the liquid at 1600 K are slightly dissimilar with the trend from the smoothed values of both, the partial and integral enthalpies of mixing. Moreover, five model parameters including two temperature-dependent parameters were used for the description of the liquid phase. The calculated partial and integral enthalpies of mixing of the liquid phase at 1600 K are shown in Figs. 8 and 9, respectively, together with the ones obtained by Wang et al. [11].

The Mn–Pr system was optimized using the experimental phase diagram of Saccone et al. [36] and the enthalpy data of Nikolaenko and Nosova [28]. First, the liquid model parameters were mostly fixed by the liquidus of Mn and the enthalpy data. Then, the Gibbs energies of the Pr BCC and Pr DHCP solid solutions and of the $Mn_{23}Pr_6$ stoichiometric compound were assessed to fit the phase diagram. The Gibbs energy of Mn in Pr DHCP structure is assessed to be 2 kJ mol^{-1} relative to the stable structure of Mn CBCC-A12 since the stable Mn DHCP is not available. As no thermodynamic data for $Mn_{23}Pr_6$ are available, the ΔH_{298} and S_{298} of the compound were determined to reproduce its dissociation temperature after the C_p was evaluated by the Neumann–Kopp rule. As seen in Figs. 7–9, the optimized phase diagram and calculated enthalpies are in good agreement with the experimental data. The calculated invariant reactions are compared with the experimental ones in Table 4.

3.4. The Mn–Nd system

The first phase diagram investigation of this system was carried out by Kirchmayr and Lugscheider [37]. Alloys made of 99.9 wt.% Mn and Nd were prepared by melting in a high frequency induction furnace using alumina crucibles. Three compounds, $Mn_{12}Nd$, $Mn_{23}Nd_6$, and Mn_2Nd were identified by means of DTA and XRD and verified by X-ray fluorescence spectrometry (XRF) and metallography. Mikhalenko and Kuz'ma [38] performed long duration annealing experiments of Mn-rich alloys characterized by XRD to determine the stability of the three compounds observed by Kirchmayr and Lugscheider. They found that $Mn_{12}Nd$ is unstable in the entire temperature range while the $Mn_{23}Nd_6$ and Mn_2Nd are stable in limited temperature ranges. Recently, Saccone et al. [39] reinvestigated the system using DTA, XRD, metallography and EPMA. The alloys were prepared from 99.9 wt.% Nd and Mn in an induction furnace with tantalum crucibles. The authors reported much lower liquidus boundaries than those determined by Kirchmayr and Lugscheider and slightly different peritectic and eutectoid decomposition temperatures for $Mn_{23}Nd_6$ and Mn_2Nd than the ones determined by Makhalenko and Kuz'ma [38]. Saccone et al. [39] proposed that Mn_2Nd and $Mn_{23}Nd_6$ form peritectically at 820 °C and 930 °C, respectively, and decompose at about 580 °C and 480 °C after analyzing the quenched samples by EPMA and corresponding powders by XRD. Preference was given to their results in the present optimization because of the higher resolution of the EPMA technique over the XRD, which was used to identify the phases in the work of Makhalenko and Kuz'ma [38]. No comprehensive study on the homogeneity ranges of Nd and Mn were performed, but Kirchmayr and Lugscheider [37] mentioned that even if they exist, they will be very small from based on their XRD analysis of Mn and Nd samples. The experimental data are shown in the phase diagram of Fig. 10.

Regarding the thermodynamic properties of Mn–Nd liquid, Ivanov et al. [14] measured the partial enthalpy of mixing of Nd between $0 < X_{Nd} < 0.25$ and that of Mn between $0.42 < X_{Nd} < 1.0$ in the Mn–Nd liquid using isoperibolic calorimetry and high purity alloys prepared from 99.95 wt.% Mn and 99.85 wt.% Nd. The

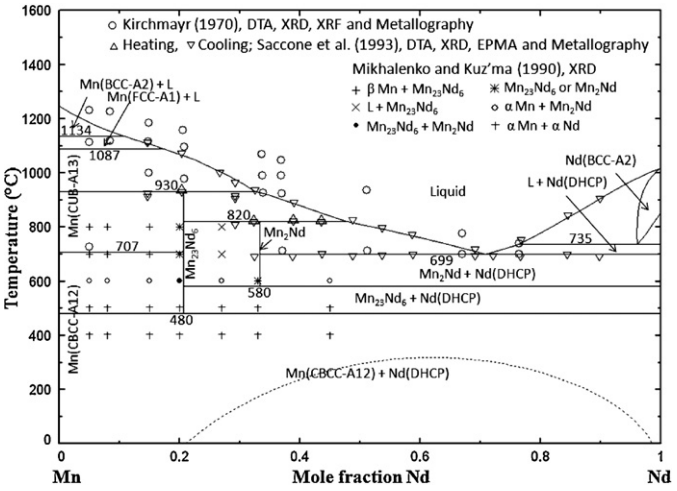

Fig. 10. The optimized phase diagram of the Mn–Nd system with experimental data [37–39].

partial enthalpy of Nd was measured using alumina crucibles for the alloys having less than 10 mol% Nd and zirconia crucibles for the alloys having up to 28 mol% Nd at 1550 K. The partial enthalpy of Mn was measured using molybdenum crucibles for the alloys having less than 10 mol% Mn and zirconia crucibles for the alloys having up to 58 mol% Mn at 1600 K. The smoothed values of both, the partial enthalpies of mixing and the integral enthalpy of mixing in the entire Mn–Nd liquid were determined by the same method used by Nikolaenko and Nosova [28] assuming that the change of partial enthalpy is negligible in the temperature range between 1550 K and 1600 K. The experimental data are shown in Figs. 11 and 12. Interestingly, the integral enthalpy of mixing of the Mn–Nd liquid vary from small negative values between 0 and about 0.25 mol fraction Nd to positive values above 0.25 mol fraction Nd. The maximum and minimum in the integral enthalpy curves are about 2 kJ mol^{-1} near 0.6 mol fraction Nd and about −0.3 kJ mol^{-1} near 0.1 mol fraction Nd, respectively. There is no thermodynamic data for the intermediate phases $Mn_{23}Nd_6$ and Mn_2Nd.

The whole system was reviewed by Okamoto [40,41] based on the phase diagram study of Kirchmayr and Lugscheider [37], Mikhsalenko and Kuz'ma [38] and Saccone et al. [39]. Since then, no thermodynamic modeling was performed on this system.

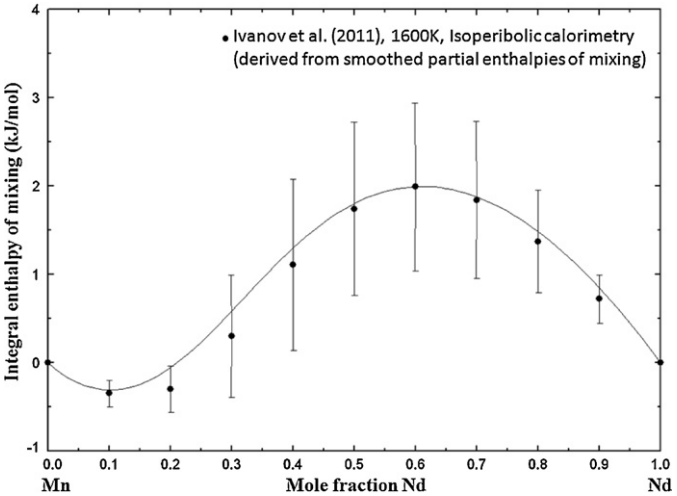

Fig. 11. Integral enthalpy of mixing in Mn–Nd liquid at 1600 K with experimental data [14].

Table 4
Calculated invariant reactions with the experimental data in the Mn–Pr system.

Type	Reaction	T (°C)	Reference
Peritectic	Mn(CUB-A13, $X_{Pr}=0$) + L($X_{Pr}=0.648$) → $Mn_{23}Pr_6$	789.9	This work
	Mn(CUB-A13, $X_{Pr}=0$) + L($X_{Pr}=0.635$) → $Mn_{23}Pr_6$	790.0	[32]
Catatectic	Pr(BCC-A2, $X_{Pr}=0.939$) → Pr(DHCP, $X_{Pr}=0.9852$) + L($X_{Pr}=0.784$)	672.4	This work
	Pr(BCC-A2, $X_{Pr}=0.94$) → Pr(DHCP, $X_{Pr}=0.985$) + L($X_{Pr}=0.758$)	665.0	[32]
Eutectic	L($X_{Pr}=0.770$) → $Mn_{23}Pr_6$ + Pr(DHCP, $X_{Pr}=0.9846$)	660.5	This work
	L($X_{Pr}=0.750$) → $Mn_{23}Pr_6$ + Pr(DHCP, $X_{Pr}=0.985$)	665.0	[32]
Eutectoid	$Mn_{23}Pr_6$ → Mn(CBCC-A12, $X_{Pr}=0$) + Pr(DHCP, $X_{Pr}=0.9852$)	649.5	This work
	$Mn_{23}Pr_6$ → Mn(CBCC-A12, $X_{Pr}=0$) + Pr(DHCP, $X_{Pr}=0.985$)	650.0	[32]

The experimental Mn liquidus determined by Saccone et al. [39] is thermodynamically more plausible than the one reported by Kirchmayr and Lugscheider [37] from the viewpoint of the limiting slope rule [42]. Moreover, the experimental data of Saccone et al. are more consistent with the stability data of intermetallics reported by Mikhalenko and Kuz'ma [38]. In the thermodynamic optimization, therefore, the phase diagram experimental data of Saccone et al. [39] were preferred over the ones of Kirchmayr and Lugscheider [37]. Although Kirchmayr and Lugscheider [37] mentioned that there is little mutual solubility of Mn and Nd, the solubility of Mn in Nd BCC-A2 is expected due to the similarity of the Mn–Nd system with the Mn–Pr one and the Mn–Nd liquidus measured by Saccone et al. [39]. A solubility of about 4 mol% Mn in Nd BCC-A2 at 736 °C was assumed in the present study. The calculated phase diagram and enthalpy curves are in good agreement with the experimental data as shown in Figs. 10–12. The thermodynamic data of the two intermetallic compounds $Mn_{23}Nd_6$ and Mn_2Nd were determined to reproduce the phase diagram data in Fig. 10 after determining their heat capacities using the Neumann–Kopp rule. The low temperature C_p of the Mn_2Nd phase measured by Kim-Ngan et al. [43], using adiabatic calorimetry, was not taken into account in the present optimization because of the insufficient temperature range (1.2–200 K). The invariant reactions of the system are compared with experimental data in Table 5. The predicted metastable liquid miscibility gap shown as a dotted line in Fig. 10 has a consolute point near 0.6 mol fraction Nd.

3.5. The Mn–Sm system

Kirchmayr and Lugscheider [37] determined the phase diagram of Mn–Sm system using DTA, XRD and XRF which are the same techniques that they used for determining the Mn–Nd system in the same study. The results are shown in Fig. 13. Two intermetallic compounds, Mn_2Sm and $Mn_{23}Sm_6$, which melt peritectically, were identified. In the solid state, the mutual solubilities of Sm and Mn were proposed to be small based on XRD data. No other phase diagram study has been carried out for this system.

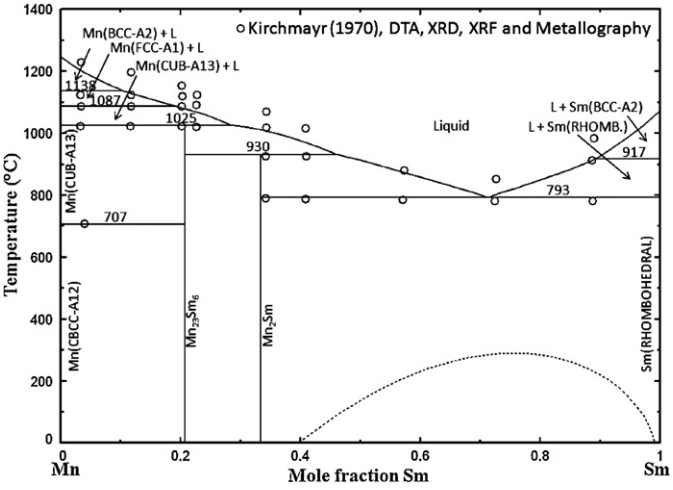

Fig. 13. The optimized phase diagram of the Mn–Sm system with experimental data [37].

Berezutskii and Ivanov [13] determined the partial and integral enthalpies of mixing of the Mn–Sm liquid using isoperibolic calorimetry. The experimental method and estimation technique used by Berezutskii and Ivanov [13] are the same as the ones used by Nikolaenko and Nosova [28]. Using high purity starting materials prepared from 99.99 wt.% Mn and 99.98 wt.% Sm, the partial enthalpies of mixing were measured at 1400 K between $0.42 < X_{Sm} < 1.0$ in molybdenum crucibles and at 1600 K between $0 < X_{Sm} < 0.28$ in alundum crucibles. Then, the smoothed values of the partial enthalpies of mixing and the integral enthalpy of mixing were determined by the same method used by Nikolaenko and Nosova [28] assuming that the change of partial enthalpy is negligible in the temperature range between 1400 K and 1600 K. The enthalpies of mixing of the liquid are depicted in Figs. 14 and 15. Like the Mn–Nd system, the integral enthalpy of mixing of Mn–Sm liquid vary from negative values between 0 and about 0.5 mol fraction Sm to positive values above 0.5 mol fraction Sm. The enthalpy curves show a maximum of about 1 kJ mol^{-1} near 0.75 mol fraction Sm and a minimum of about −0.8 kJ mol^{-1} near 0.1 mol fraction Sm. Using high-temperature isoperibolic calorimetry, Shilov et al. [44] determined the enthalpy of formation of $Mn_{23}Sm_6$ at 1320 K to be -92 ± 5 kJ mol^{-1}; unfortunately, no data are available for Mn_2Sm.

The system was previously optimized by Wang et al. [12] based on the work of Kirchmayr and Lugscheider [37] using the Bragg–Williams random mixing model with the Redlich–Kister expression for the liquid phase. As shown in Figs. 14 and 15, the integral and partial enthalpies of mixing of the liquid at 1600 K

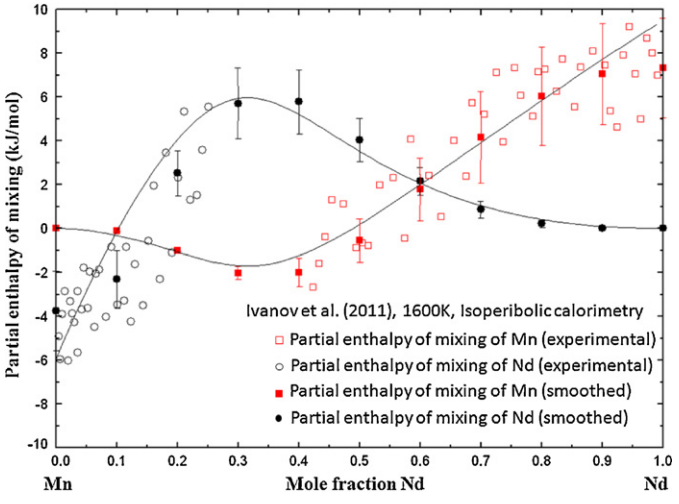

Fig. 12. Partial enthalpies of mixing in Mn–Nd liquid at 1600 K with experimental data [14].

Table 5
Calculated invariant reactions with the experimental data in the Mn–Nd system.

Type	Reaction	T (°C)	Reference
Peritectic	Mn(CUB-A13, $X_{Nd}=0$) + L($X_{Nd}=0.327$) → $Mn_{23}Nd_6$	930.0	This work
	Mn(CUB-A13, $X_{Nd}=0$) + L($X_{Nd}=0.283$)[a] → $Mn_{23}Nd_6$	1100.0	[34]
	Mn(CUB-A13, $X_{Nd}=0$) + L($X_{Nd}=0.325$) → $Mn_{23}Nd_6$	930.0	[36]
Peritectic	$Mn_{23}Nd_6$ + L($X_{Nd}=0.478$) → Mn_2Nd	820.1	This work
	$Mn_{23}Nd_6$ + L($X_{Nd}=0.448$) → Mn_2Nd	975.0	[34]
	$Mn_{23}Nd_6$ + L($X_{Nd}=0.488$) → Mn_2Nd	820.0	[36]
Catatectic	Nd(BCC-A2, $X_{Nd}=0.96$) → Nd(DHCP, $X_{Nd}=1$) + L($X_{Nd}=0.763$)	734.9	This work
Eutectic	L($X_{Nd}=0.708$) → Mn_2Nd + Nd(DHCP, $X_{Nd}=1$)	699.4	This work
	L($X_{Nd}=0.749$) → Mn_2Nd + Nd(DHCP, $X_{Nd}=1$)	700.0	[34]
	L($X_{Nd}=0.730$) → Mn_2Nd + Nd(DHCP, $X_{Nd}=1$)	695.0	[36]
Eutectoid	Mn_2Nd → $Mn_{23}Nd_6$ + Nd(DHCP, $X_{Nd}=1$)	580.4	This work
	Mn_2Nd → $Mn_{23}Nd_6$ + Nd(DHCP, $X_{Nd}=1$)	580.0	[36]
Eutectoid	$Mn_{23}Nd_6$ → Mn(CBCC-A12, $X_{Nd}=0$) + Nd(DHCP, $X_{Nd}=1$)	480.4	This work
	$Mn_{23}Nd_6$ → Mn(CBCC-A12, $X_{Nd}=0$) + Nd(DHCP, $X_{Nd}=1$)	480.0	[36]

[a] Note that the liquid composition determined in the experimental study [34] is less reliable (see the text for more details).

optimized by Wang et al. [12] are significantly off the recent experimental data of Berezutskii and Ivanov [13].

Like for the Mn–Nd system, the Mn liquidus reported by Kirchmayr and Lugscheider [37] is thermodynamically the less reasonable. Consequently in the present optimization, the assessed Mn liquidus was lowered to be thermodynamically more reasonable from the viewpoint of the limiting slope rule [42]. For the phases Mn_2Sm and $Mn_{23}Sm_6$, who melt peritectically, no other data than the ones of Kirchmayr and Lugscheider [37] exist and we had no other choice than to use their data. The enthalpy of mixing of the liquid, determined by Berezutskii and Ivanov [13], was taken into account to determine the model parameters of liquid phase. The enthalpy of formation of $Mn_{23}Sm_6$ measured by Shilov et al. [44] (-92 ± 5 kJ mol^{-1}) was relatively well reproduced in the present optimization (-91.3 kJ mol^{-1}). The calculated invariant reactions are compared with experimental ones in Table 6. Although the enthalpy data shown in Figs. 14 and 15 are well reproduced in the present optimization, the calculated phase diagram is in less agreement with the experimental data of Kirchmayr and Lugscheider [37] due to the above-mentioned possible error in the experiments. In order to validate the present thermodynamic optimization or obtain a more accurate thermodynamic optimization of the system, new phase diagram experiments are clearly needed.

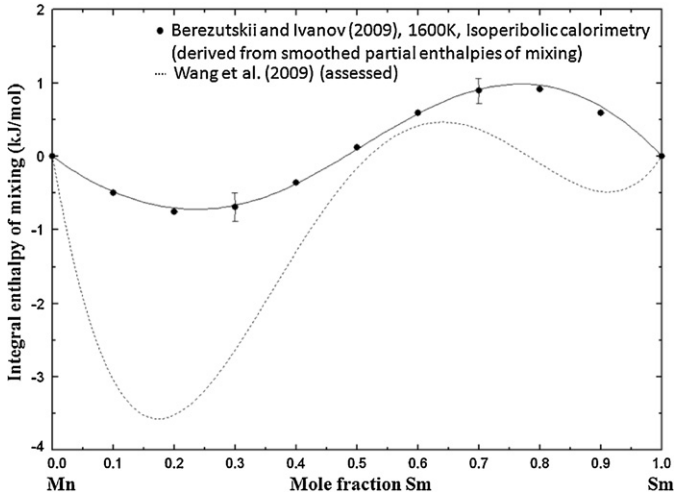

Fig. 14. Integral enthalpy of mixing in liquid Mn–Sm alloys at 1600 K with experimental data [13]. The dotted line is from the previous optimization of Wang et al. [12].

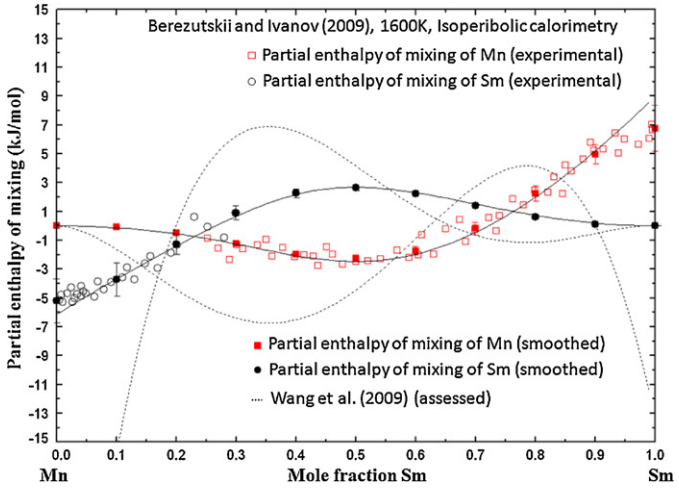

Fig. 15. Partial enthalpies of mixing in Mn–Sm liquid at 1600 K with experimental data [13]. The previous optimization of Wang et al. [12] is shown by the dotted line.

4. Systematic analysis of Mn–light RE systems

It is shown that the available and reliable experimental data of Mn–light RE systems are consistently reproduced by the present optimizations in all the systems. As it is well known, the RE metals across the lanthanide series show regular changes in electronic (electronegativity) and physical properties such as the melting temperature, the atomic radius and the density, with an increase of the atomic number. It is therefore expected that certain trends exist as well in the thermodynamic properties and phase relationships of the Mn–RE binary systems.

In the course of the present study, it is found that the enthalpies of mixing in liquid Mn–RE (RE = La, Ce, Pr, Nd and Sm) follow such trends, as shown in Fig. 16. The calculated and experimental integral enthalpies of mixing of liquid Mn–RE solutions at 1600 K are gradually changed from positive to negative values from La to Sm. The light RE elements, except La, are metallic elements which are characterized by the filling of f orbital. By filling the f orbital in atomic number order, the attractive interaction between Mn and RE elements seems to become stronger with a minimum between 0.3 and 0.4 mol fraction RE. The asymmetry observed in the enthalpies of mixing curves comes possibly from the size difference between Mn and RE. That is, RE has a larger atomic size (180 pm for Sm ~ 188 pm for La) than Mn (130 pm) [45]. Consequently, the negative interaction between Mn and RE can naturally induce the short range ordering of Mn and RE near the Mn-rich side, which produces the slight negative deviation observed in the Mn-rich region. Likewise, the calculated entropies of mixing in liquid Mn–RE alloys at 1600 K shown in Fig. 17 are also gradually changed

Table 6
Calculated invariant reactions with the experimental data in the Mn–Sm system.

Type	Reaction	T (°C)	Reference
Peritectic	Mn(CUB-A13, $X_{Sm}=0$) + L($X_{Sm}=0.289$) → $Mn_{23}Sm_6$	1025.3	This work
	Mn(CUB-A13, $X_{Sm}=0$) + L($X_{Sm}=0.411$)[a] → $Mn_{23}Sm_6$	1025.0	[34]
Peritectic	$Mn_{23}Sm_6$ + L($X_{Sm}=0.471$) → Mn_2Sm	930.1	This work
	$Mn_{23}Sm_6$ + L($X_{Sm}=0.531$) → Mn_2Sm	930.0	[34]
Eutectic	L($X_{Sm}=0.718$) → Mn_2Sm + Sm(DHCP, $X_{Sm}=1$)	792.8	This work
	L($X_{Sm}=0.678$) → Mn_2Sm + Sm(DHCP, $X_{Sm}=1$)	795.0	[34]

[a] Note that the liquid composition determined in the experimental study [34] is less reliable (see the text for more details).

from positive to negative deviation from the ideal entropy of mixing (dotted curve). The lesser entropies near 0.3–0.4 mol fraction RE support the gradual change of enthalpies with increasing the RE atomic number. These thermodynamic properties are also reflected in the phase diagrams. From the assessed phase diagram of each system (Figs. 1, 4, 7, 10 and 13), it is clearly seen that the stability of solid intermetallic phases in the systems increases with increasing the RE atomic number, especially near 0.3 and 0.4 mol fraction RE. No stable intermetallic compounds appear in the Mn–La and Mn–Ce systems. Stable compounds appear from the Mn–Pr system ($Mn_{23}Pr_6$) and become stable at lower temperature with increasing the atomic number ($Mn_{23}Sm_6$ and Mn_2Sm). The change of hypothetical liquid miscibility gap (dotted curve) also shows the trend of increasing stability in liquid phases with RE atomic order. These interesting trends and regularities are also successively found in the Mn-heavy RE (Gd, Tb, Dy, Ho, Er, Tm, Lu and Y) systems [46].

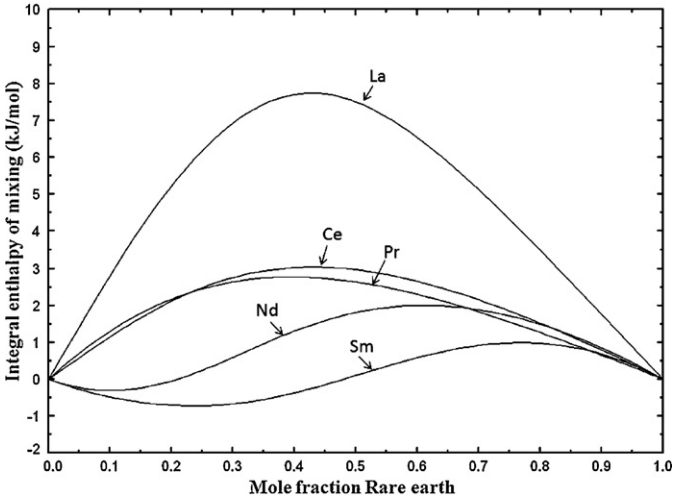

Fig. 16. Calculated enthalpies of mixing in Mn–RE (La, Ce, Pr, Nd and Sm) liquid at 1600 K.

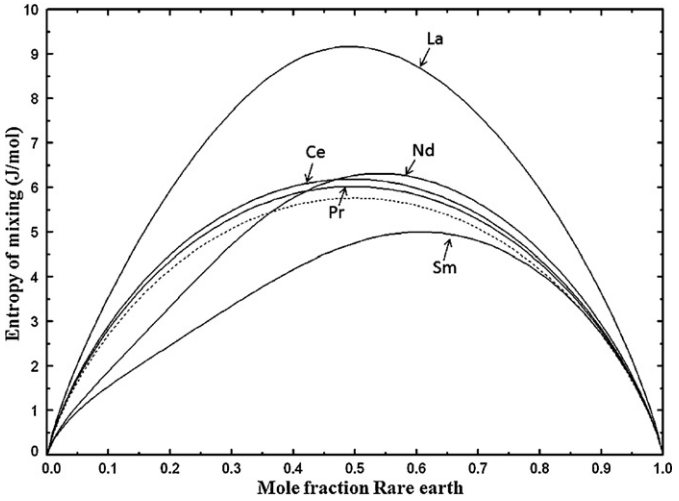

Fig. 17. Calculated entropies of mixing in Mn–RE (La, Ce, Pr, Nd and Sm) liquid at 1600 K. The dotted line represents the ideal entropy of mixing.

5. Summary

Critical evaluation and optimization of all available phase diagram and thermodynamic data for the Mn–RE (RE = La, Ce, Pr, Nd and Sm) systems have been conducted to obtain reliable thermodynamic functions of all the phases in the system. The thermodynamic properties of liquid phase were described using the Modified Quasichemical Model and the solid solution phases such as bcc, fcc, cubic and dhcp were described using the one-sublattice Compound Energy Formalism. The magnetic properties of solid phases were also taken into account.

In the thermodynamic modeling, it is found that the Mn–RE systems show systematic changes in the phase diagrams and thermodynamic properties such as enthalpy of mixing in liquid state in the order of periodic number in the lanthanide series. With increase of periodic number of light RE elements, the interaction between atoms in the liquid becomes more negative and promotes the formation of stable intermetallic compounds. This systematic thermodynamic modeling approach for all light RE elements can also allow to resolve inconsistencies in the experimental data in particular for the Mn–Sm system.

Acknowledgement

This project was supported by the National Sciences and Engineering Research Council of Canada (NSERC) Collaborative Research and Development grant and General Motors of Canada.

References

[1] N. Stanford, D. Atwell, A. Beer, C. Davies, M.R. Barnett, Scr. Mater. 59 (2008) 772–775.
[2] N. Stanford, Mater. Sci. Eng. A 527 (2010) 2669–2677.
[3] S. Sandloebes, S. Zaefferer, I. Schestakow, S. Yi, R. Gonzalez-Martinez, Acta Mater. 59 (2010) 429–439.
[4] H. Yan, S.W. Xu, R.S. Chen, S. Kamado, T. Honma, E.H. Han, Scr. Mater. 64 (2010) 141–144.
[5] S.A. Farzadfar, M. Sanjari, I.-H. Jung, E. Essadiqi, S. Yue, Mater. Sci. Eng. A 528 (2011) 6742–6753.
[6] Y.-B. Kang, C. Aliravci, P.J. Spencer, G. Eriksson, C.D. Fuerst, P. Chartrand, A.D. Pelton, JOM 61 (2009) 75–82.
[7] L. Jin, Y.-B. Kang, P. Chartrand, C.D. Fuerst, CALPHAD 34 (2010) 456–466.
[8] L. Jin, Y.-B. Kang, P. Chartrand, C.D. Fuerst, CALPHAD 35 (2011) 30–41.
[9] C. Tang, Y. Du, L. Zhang, H. Xu, Z. Zhu, J. Alloys Compd. 437 (2007) 102–106.
[10] Y.-B. Kang, A.D. Pelton, P. Chartrand, P. Spencer, C.D. Fuerst, J. Phase Equilib. Diff. 28 (2007) 342–354.
[11] C.P. Wang, Z. Lin, X.J. Liu, J. Alloys Compd. 469 (2009) 123–128.
[12] C.P. Wang, H.L. Zhang, S.L. Wang, Z. Lin, X.J. Liu, A.T. Tang, F.S. Pan, J. Alloys Compd. 481 (2009) 291–295.
[13] V.V. Berezutskii, M.I. Ivanov, Powder Metall. Met. Ceram. 48 (2009) 454–461.
[14] M. Ivanov, V. Berezutski, N. Usenko, Int. J. Mater. Res. 102 (2011) 277–281.
[15] A.D. Pelton, S.A. Degterov, G. Eriksson, C. Robelin, Y. Dessureault, Metall. Mater. Trans. B 31 (2000) 651–659.
[16] A.D. Pelton, P. Chartrand, Metall. Mater. Trans. A 32 (2001) 1355–1360.
[17] I.-H. Jung, D.H. Kang, W.J. Park, N.J. Kim, S. Ahn, CALPHAD 31 (2007) 192–200.
[18] D. Nassyrov, I.-H. Jung, CALPHAD 33 (2009) 521–529.

[19] A.D. Pelton, M. Blander, Metall. Trans. B 17 (1986) 805–815.
[20] P. Wu, G. Eriksson, A.D. Pelton, M. Blander, ISIJ Int. 33 (1993) 26–35.
[21] A.D. Pelton, M. Blander, Metall. Soc. AIME, Lake Tahoe, NV (1984) 281–294.
[22] M. Hillert, B. Jansson, B. Sundman, Z. Metallkd. 79 (1988) 81–87.
[23] A.T. Dinsdale, CALPHAD 15 (1991) 317–425.
[24] G. Inden, Project Meeting CALPHAD V, Max-Planck-Inst. Eisenforschung, G.m.b.H., Dusseldorf, Germany, 1976, p. 111.
[25] M. Hillert, M. Jarl, CALPHAD 2 (1978) 227–238.
[26] C.W. Bale, E. Belisle, P. Chartrand, S.A. Decterov, G. Eriksson, K. Hack, I.-H. Jung, Y.-B. Kang, J. Melancon, A.D. Pelton, C. Robelin, S. Petersen, CALPHAD 33 (2009) 295–311.
[27] L. Rolla, A. Iandelli, Ber. Dtsch. Chem. Ges. 75B (1942) 2091–2095.
[28] I.V. Nikolaenko, V.V. Nosova, Rasplavy (1993) 76–79.
[29] A. Palenzona, S. Cirafici, Bull. Alloy Phase Diagrams 11 (1990) 491–493.
[30] A. Iandelli, Atti Accad. Naz. Lin. 13 (1952) 265–268.
[31] M.S. Mirgalovskaya, I.A. Strel'nikova, Tr. Inst. Metall. Akad. Nauk SSSR (1957) 135–138.
[32] B.J. Thamer, J. Less-Common Met. 7 (1964) 341–346.
[33] C. Tang, Y. Du, H. Xu, S. Hao, L. Zhang, J. Min. Metall. Sect. B 43 (2007) 21–28.
[34] A. Palenzona, S. Cirafici, J. Phase Equilib. 17 (1996) 53–56.
[35] H. Okamoto, J. Phase Equilib. Diff. 29 (2008) 381–382.
[36] A. Saccone, S. Delfino, R. Ferro, J. Less-Common Met. 108 (1985) 89–105.
[37] H.R. Kirchmayr, W. Lugscheider, Z. Metallkd. 61 (1970) 22–23.
[38] S.I. Mikhalenko, Y.B. Kuz'ma, Izv. Akad. Nauk SSSR Neorg. Mater. 26 (1990) 2432–2433.
[39] A. Saccone, S. Delfino, R. Ferro, Z. Metallkd. 84 (1993) 563–568.
[40] H. Okamoto, J. Phase Equilib. 13 (1992) 331–332.
[41] H. Okamoto, J. Phase Equilib. 15 (1994) 568–569.
[42] A.D. Pelton, Ber. Bunsen. Phys. Chem. 84 (1980) 212–218.
[43] N.H. Kim-Ngan, F.F. Bekker, P.E. Brommer, J.J.M. Franse, Physica B 160 (1990) 388–392.
[44] A.L. Shilov, L.N. Padurets, M.E. Kost, Zh. Fiz. Khim. 57 (1983) 555–560.
[45] W.B. Pearson, The Crystal Chemistry and Physics of Metals and Alloys, Wiley-Interscience, New York, 1972.
[46] J. Kim, I.-H. Jung, Critical systematic evaluation and thermodynamic optimization of the Mn–RE system: RE = Gd, Tb, Dy, Ho, Er, Tm, Lu, Y and Sc, unpublished work.
[47] K.H.J. Buschow, Rep. Prog. Phys. 40 (1977) 1179–1256.